Chapter 3

EXPERIMENTAL SETUP AND PROCEDURE

In the present study, an incident thermal pulse onto a He II-vapor interface as a heat source for evaporation is generated by Joule heating from a planar heater, the heat flux from which varies with time in a form of trapezoid, and develops into a shock wave at the front in the very early stage of propagation. It propagates upward through He II and finally impinges on an interface to cause evaporation. Some portion of the imping-

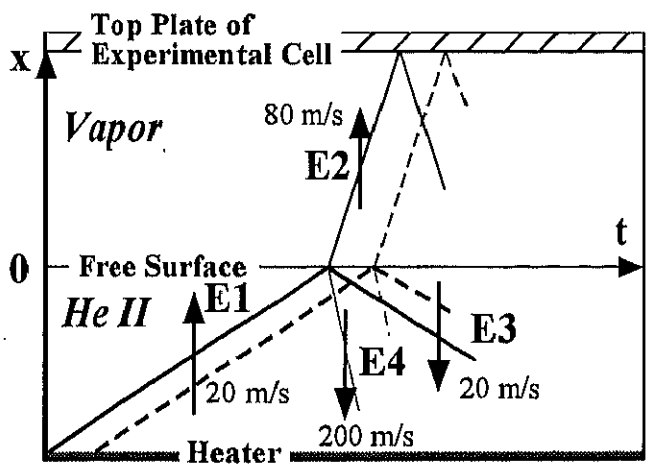

Fig. 3.1: The x-t diagram of He II evaporation induced by a thermal pulse impingement. The solid and broken lines indicate the wave front and its tail. $E1$: the impinging thermal pulse, $E2$: the evaporation wave, $E3$: the reflected thermal pulse, $E4$: the generated 1st sound wave

ing thermal pulse is reflected to propagate downward through He II again as a thermal pulse. After that, an evaporation wave propagates through the quiescent vapor as a compression wave. The contact region separating compressed the background vapor in the evaporation wave from the evaporated vapor develops between the interface and the evaporation wave at far slower speed than an evaporation wave. The x-t diagram of this evaporation process is shown in Fig. 3.1. In the vapor phase, the time variations of the pressure and the temperature are measured with a pressure transducer and a superconductive temperature sensor. The propagation speed of an evaporation wave front is also measured with a double probe type superconductive temperature sensor. In the He II phase the temperature variation resulting from the impinging and reflected thermal pulses is measured with a superconductive temperature sensor, from which the temperature variation at the free surface can be derived as the boundary condition for evaporation process. In addition to these measurements, the whole evaporation process is visualized with the aid of a laser holographic interferometer.

3.1 Pressure and Temperature Measurements

3.1.1 He II dewar and evacuation system

The photo of whole experimental setup of the temperature and the pressure measurements is shown in Fig. 3.2. In these measurements, a cryostat of the glass dewar type is utilized. Fig. 3.3 indicates the schematic illustration of the dewar, one is set inside of the other, and the evacuation system. The dewar is a cylindrical glass container having evacuated between the double walled space for thermal insulation. And also the inside wall is silvered to reduced radiation heat input from outside environment. Narrow unsilvered slit of a $10\,mm$ in width is made on both side of wall from top to bottom for direct visual observation. He II is contained in inner dewar. Liquid nitrogen inside of the outer dewar reduces the direct incident of thermal radiation from ambient temperature environment to

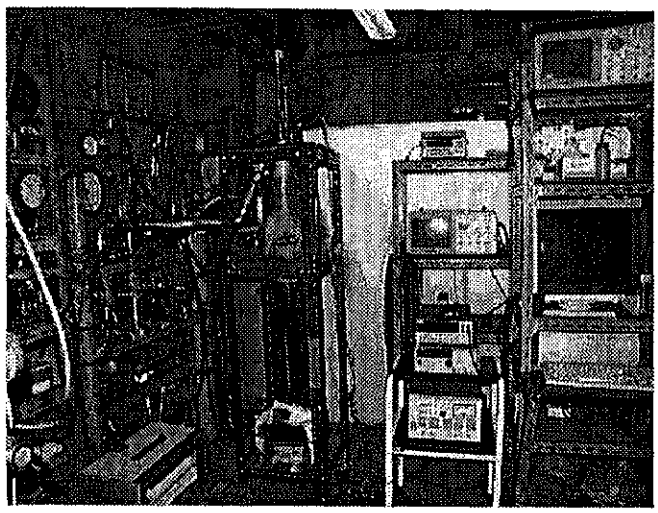

Fig. 3.2: General view of whole experimental setup

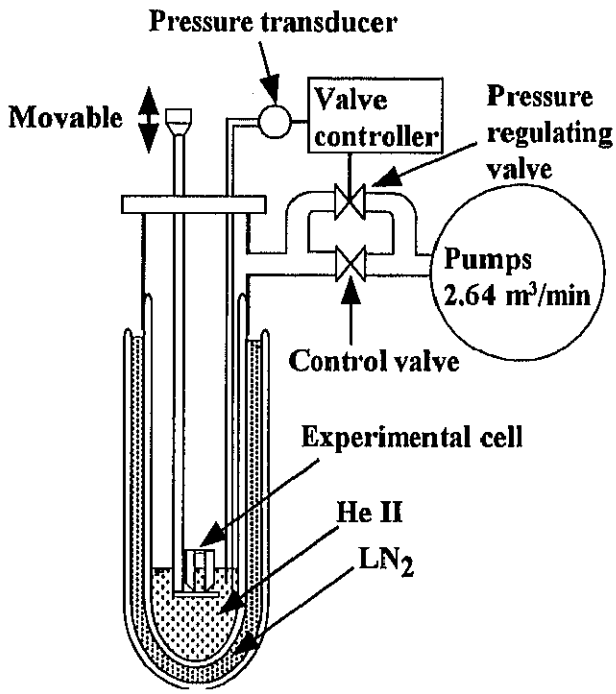

Fig. 3.3: Schematical drowing of a glass dewar and a evacuation system

He II. Experimental apparatus is set a stainless tube from the flange which is supported on the top of He II dewar.

The vapor pressure in helium dewar is fine-controlled with the pressure regulating valve so as to keep the He II bath temperature constant

during each experimental run (temperature accuracy $\Delta T_0 = \pm 0.5\,mK$, time constant $\tau = 300\,s$). The control system consists of a PID controller, a control valve actuated by a stepper-motor and a capacitance-type high precision pressure transducer (MKS INSTRUMENT INC.). He II dewar is connected to three mechanical vacuum pumps. The total evacuation speed of pumps is $2.64\,m^3/min$.

3.1.2 Experimental cell

The main assembly of the experimental section to be set in the He II dewar is schematically shown in Fig. 3.4. In the He II evaporation experiment, the experimental cell where a thermal pulse and evaporation wave propagates is a rectangular solid, a width of $20\,mm$, a height of $30\,mm$ and a length of $30\,mm$. The experimental cell is composed of four adiabatic side walls and an adiabatic top plate of Bakelite. A planar Nichrom thin film heater ($30\,\Omega$) vacuum-deposited on a quartz glass substrate is located at the bottom of the cell. For generating a thermal pulse, electric current in a trapezoidal (or square) form varying with time is applied to the heater for several hundred micro sec. ($= t_H$). A pressure transducer and

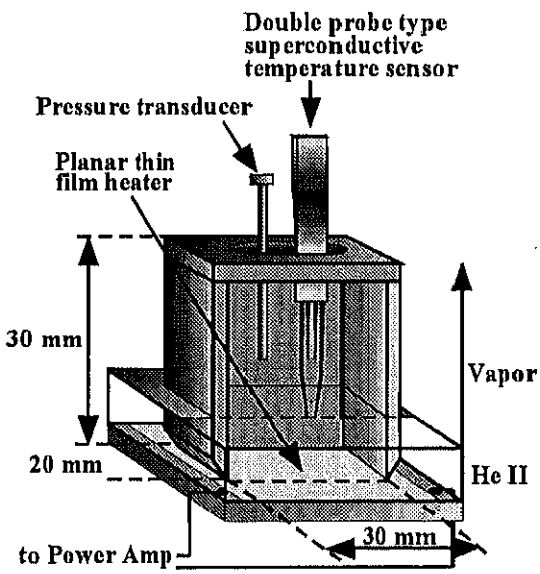

Fig. 3.4: The main assembly of experimental section to be set in the He II dewar.

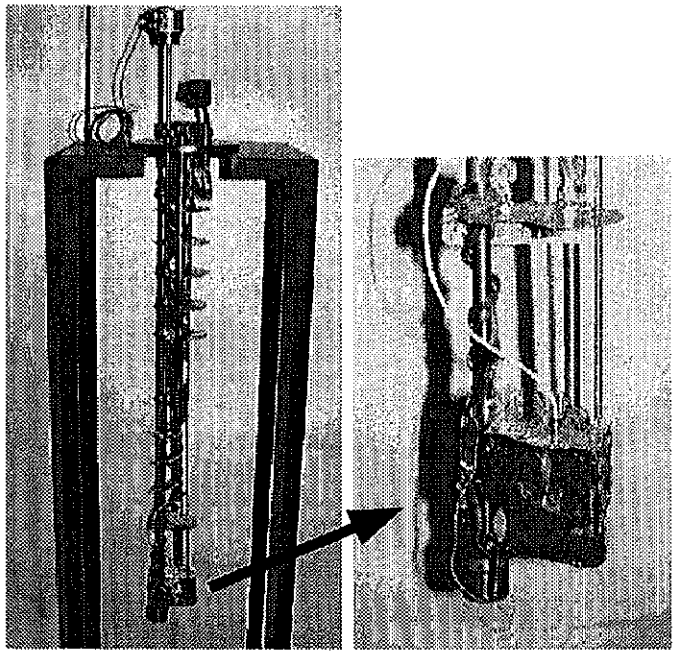

a) b)

Fig. 3.5: The photos of the main assembly of experimental section. a): the photo of the cryogenic flange inserted into He II dewar, b): the photo of the experimental cell surrounded by aluminum foil.

a superconductive temperature sensor are inserted into the experimental space through the top plate of the cell. The whole cell assembly is further surrounded by aluminum foil to shield it from $300\,K$ thermal radiation parasitic heat and to ensure temperature uniformity in the inside volume as shown in Fig. 3.5, where a nearly thermodynamic equilibrium state between He II and vapor is established as indicated in Fig. 3.6. It is installed in the He II glass dewar. It is confirmed that the maximum temperature variation in experimental space is less than one mK during an experimental run. The He II level in the cell can be adjusted by moving the cell vertically.

The same experimental cell is utilized for He II condensation experiment. But the top plate of experimental cell is set a wall mount type pressure transducer.

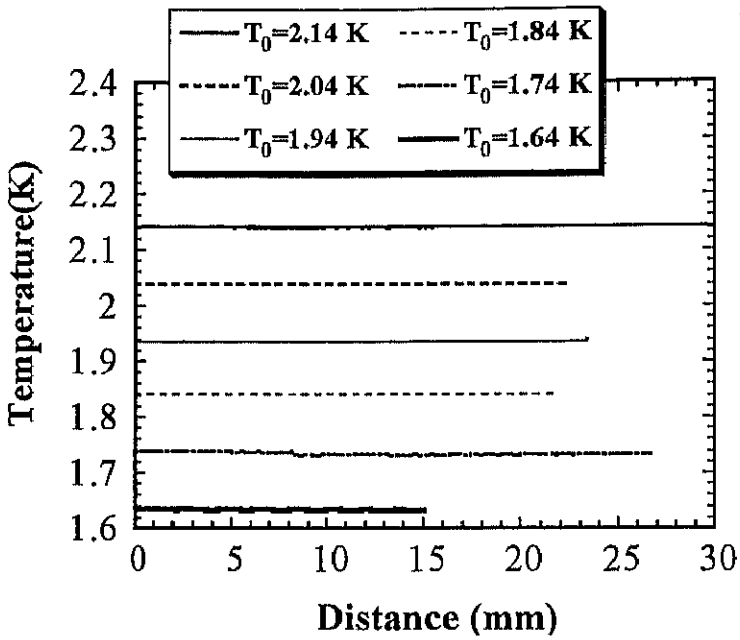

Fig. 3.6: The temperature distribution in vapor phase. The temperature is measured with a CERNOX temperature sensor that is a diode type temperature sensor. The x-axis is the distance from a free surface.

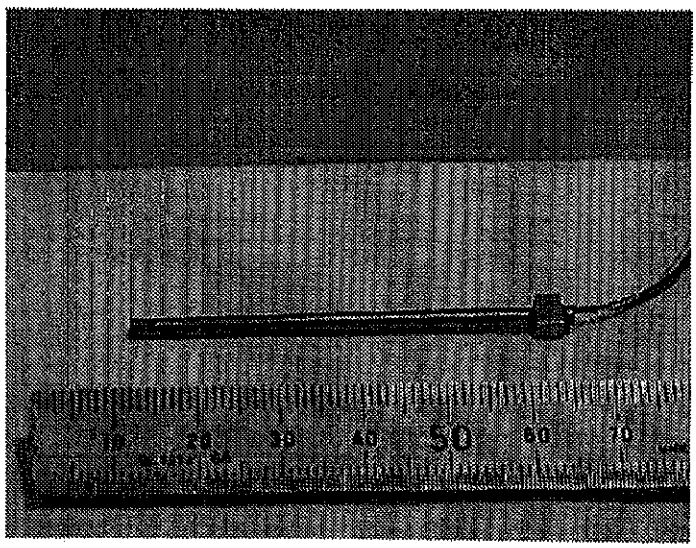

Fig. 3.7: The photo of a probe type pressure transducer.

3.1.3 Pressure transducer

It is found that a commercially available piezo pressure transducers (KULITE INC.: absolute pressure measurement type, CCQ-093 and CT-

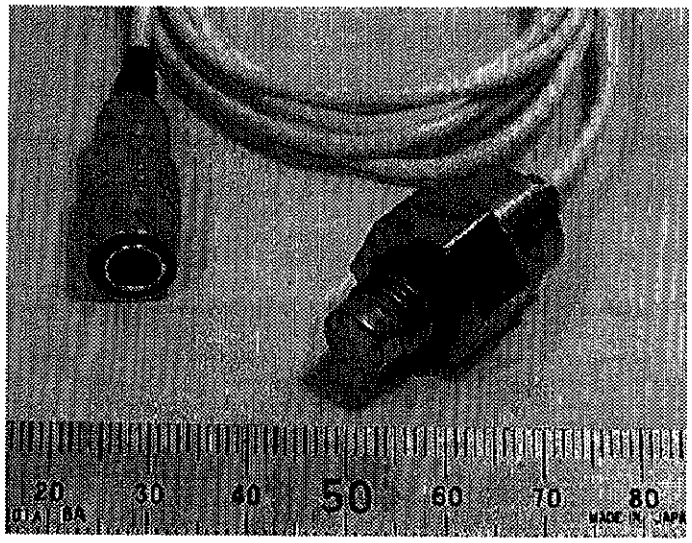

Fig. 3.8: The photo of a wall mount type pressure transducer.

375) can be utilized in He II. The sensing element is a silicon diaphragm onto which a micro Wheatstone bridge is bonded. Three pressure transducers with different mounting configuration are used. One of them, a slender cylinder in shape, as shown in Fig. 3.7. The diameter of the sensing element tip is $2.4\,mm$ and the length of the probe is $50\,mm$. One of the other, of a wall mount type with the diameter of which is $8\,mm$, is set at the center of the cell top plate with the sensing element surface flat to

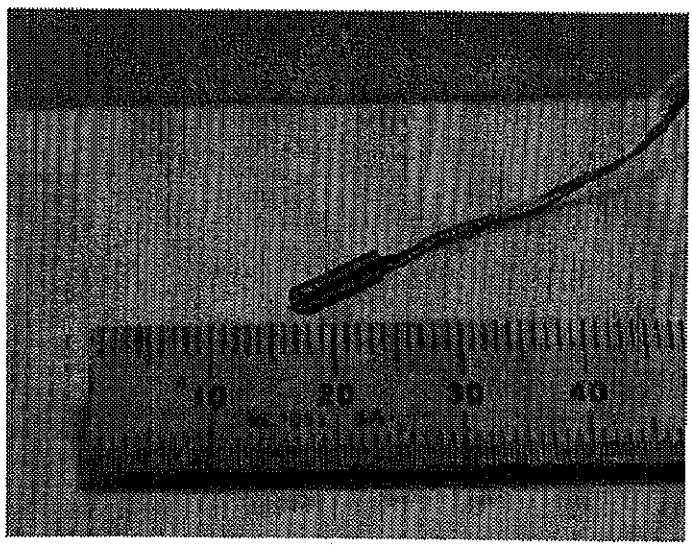

Fig. 3.9: The photo of a miniture type pressure transducer.

the top plate as shown in Fig. 3.8. The other, of a miniature type with a diameter of sensing element tip is $2.4\,mm$ and a length is $9.5\,mm$ as shown in Fig. 3.9. These transducers have the same performance. The response time is very short, shorter than a few μs, and the sensitivity is as large as $1.35\,\mu V/Pa$ in He II environment with the accuracy of about $\pm 5\,\%$. The in-house calibration of the transducer is conducted by varying the saturated vapor pressure of He II.

3.1.4 Superconductive temperature sensor

Fig. 3.10 shows a superconductive temperature sensor with bent needle supports. The configuration of a superconductive temperature sensor quite resembles a conventional hot wire probe in shape to be used for the flow velocity measurement in aerodynamic experiments. Fig. 3.11 shows the schematic illustration of the superconductive temperature sensor element. This type of superconductive temperature sensor had been originally developed by Borner et al.[48], and was modified by Schwerdtner et al.[49] and by Shimazaki et al.[47]. The sensing element is composed of gold-tin superconductive thin film, which is vacuum deposited onto the outer sur-

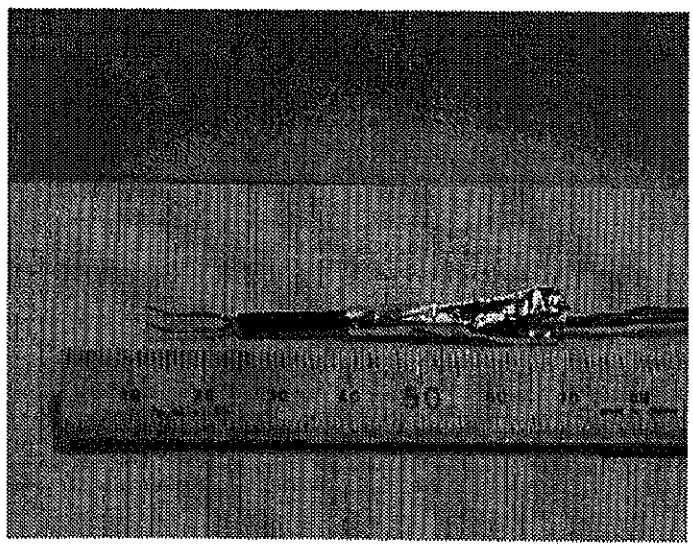

Fig. 3.10: The photo of a superconductive temperature sensor with the bent needle sports.

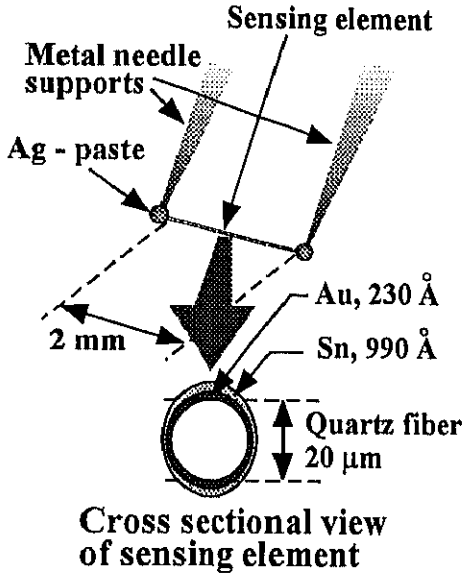

Fig. 3.11: The sensing element of a superconductive temperature sensor.

face of a fine quartz fiber of about 20 μm in diameter and about 2 mm long (or a carbon fiber of about 5 μm). The thicknesses of gold and tin films are 230 $\AA$ and 990 $\AA$ respectively. The double probe type superconductive temperature sensor depicted in Fig. 3.4 and pictured in Fig. 3.12 has two sensing elements, which are separated by 9.72 mm for the measurement of propagation speed of an evaporation wave. The temperature variation is detected through the abrupt change of the electric resistance of the sensing element due to the superconductive to normal state transition. The transition temperature range can be adjusted to that of He II temperature by controlling the film thickness ratio of gold and tin. Further fine adjustment of the working temperature is achieved by varying the applied bias electric current to the sensor. Fig. 3.13 shows a typical static voltage-current characteristic of the sensor taking the temperature as a parameter. The voltage drop across the sensing element is measured while gradually increasing the biased current I with keeping the temperature constant. The each curve goes horizontally from the origin until the bias current reaches a critical value which depends on the temperature. When the current reaches the critical value, the curve starts to rise. Generally, the critical value became

larger for the lower temperature. The current at which the variation of the voltage drop with the temperature increase is steepest is selected as the optimum bias current. The response time of the sensor is found to be very short, at the largest several μs, due to very small heat capacity of the sensing element. The sensor is calibrated not only statically but also dynamically for high accuracy. The static calibration is conducted by quite slowly varying the temperature of He II with a vapor pressure control device. In the dynamic calibration, a weak thermal pulse of which heat flux supplied from heater q is $5\,W/cm^2$ or less and heating duration time t_H is as short as $100\,\mu s$ is emitted from the planar heater as a reference signal, and is detected by an uncalibrated sensor fixed at a small distance of about $10\,mm$ from the heater. A weak and short pulse and the small distance are all necessary conditions to avoid the effect of wave form deformation due to excessive non-linear effect during propagation and the effect of quantized vortices. The detected signal is compared with the theoretical temperature variation to yield the calibration coefficient. The theoretical temperature amplitude of a thermal pulse, ΔT_{th}, is obtained on the basis of the linear acoustic theory for second sound as

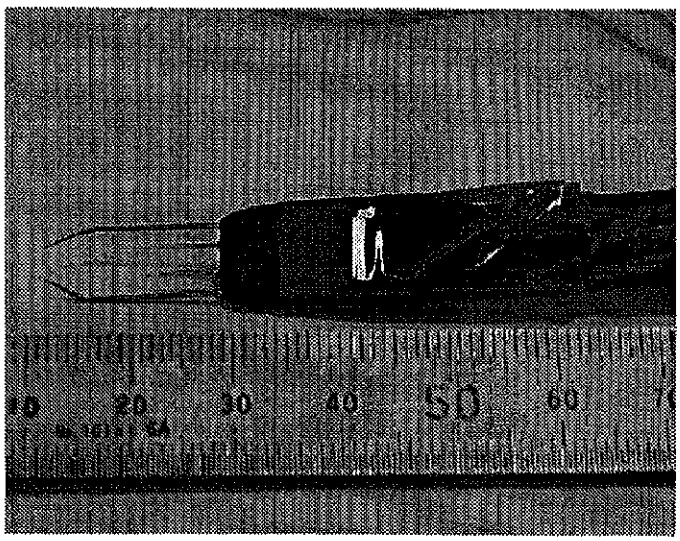

Fig. 3.12: The photo of a double probe type superconductive temperature sensor.

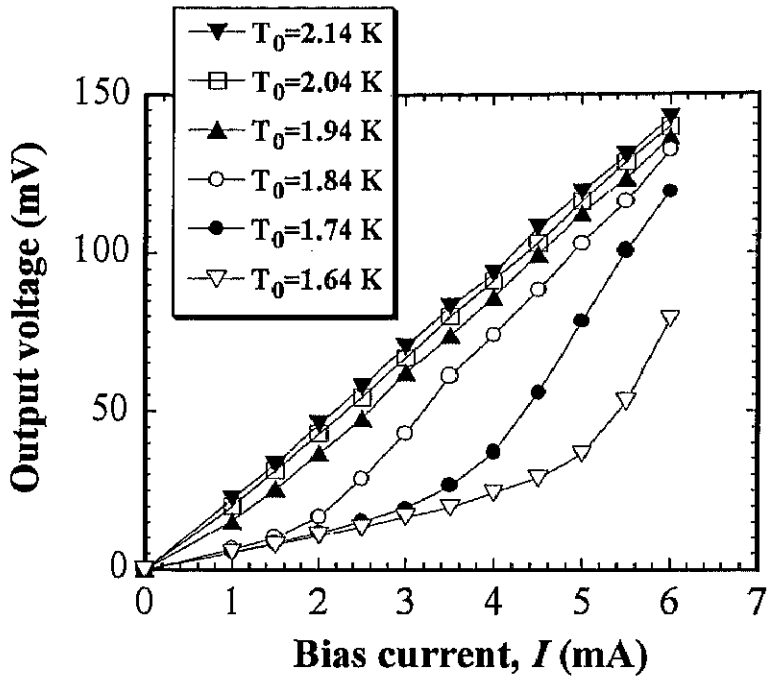

Fig. 3.13: The typical voltage-bias current characteristics of a superconductive temperature sensor. Temperature is taken as a parameter.

$$\Delta T_{th} = q/(\rho_0\, a_{20}\, c_P), \tag{3.1}$$

where ρ_0 and c_P are the density and the heat capacity of He II at the temperature T_0, a_{20} is the propagation speed of second sound wave at T_0, and q is the heat flux measured in the plateau portion of thermal pulse. The calibration coefficient χ is obtained as follows

$$\chi = \Delta V/\Delta T_{th}, \tag{3.2}$$

where ΔV is the detected voltage difference increment across the sensing element. The sensitivity is as large as $100\,\mu V/mK$, although it depends on the temperature and applied bias current. The calibration coefficient for the vapor temperature measurement is confirmed to be basically the same as that for He II measurement under the same thermal condition. In the case of applications in the vapor temperature measurement, the sensing element is usually covered with superfluid thin film, which leads to some measurement error in the measurement because of evaporation of

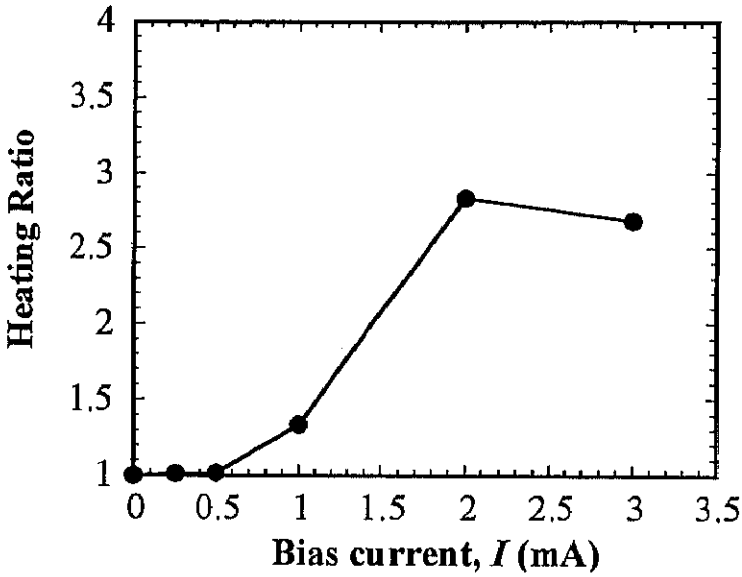

Fig. 3.14: The heating ratio of the electric resistance of sensing element of a superconductive temperature sensor as a function of the bias current. The heating ratio is defined as a fraction of the electric resistance of sensing element in vapor phase divided by that electric resistance in He II.

superfluid film. However, in our experiment, as superfluid film is eliminated by self heating of the sensor element (order of a few micro Watt), the sensor element keeps a good thermal coupling with vapor to minimize the error. Of course, excessively large bias current would cause temperature rise of the sensor itself and would even heat up vapor around it, which may result in large error in the measurement. Fig. 3.14 shows the heating ratio of the electric resistance of sensing element in between He II and vapor as a function of the bias current. The heating ratio is defined as a fraction of the electric resistance of sensing element in vapor divided by that resistance in He II. At the unity region of heating ratio, the calibration coefficient χ_v in vapor is same calibration coefficient χ in He II.

3.1.5 Procedure

The block diagram of temperature measurement is shown in Fig. 3.15. The measurements is started after He II temperature in the bath reaches a

specified equilibrium state. A thermal pulse is generated by pulsed heating from the heater, propagating upward and incident on a free surface. A impinging thermal pulse on and a reflected thermal pulse from He II free surface are measured by superconductive sensor. The detected signal of temperature measurement is amplified 100 times with the aid of a low noise preamplifier (NF ELECTRONIC INSTRUMENTS CO. LTD.) and is then acquired with a digital storagescope (IWATSU ELECTRIC CO. LTD.: DS9121).

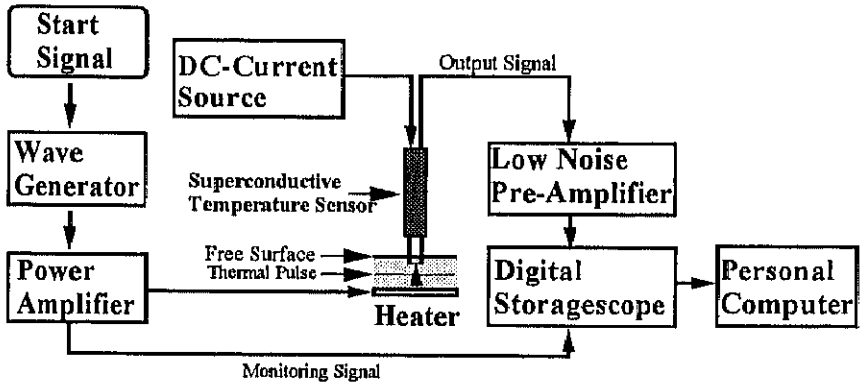

Fig. 3.15: The block diagram of the temperature measurement.

The block diagram of pressure measurement is shown in Fig. 3.16. After the incidence of a thermal pulse on He II free surface, an evaporation wave is produced. The evaporation wave is detected by a pressure transducer. The detected signal of the pressure measurement is amplified 330 times with the aid of a liner-preamplifier (UNIPULSE CO. LTD.: AM30) and is then acquired with a digital storagescope. All digital data are transmitted to a personal computer to be stored on a floppy disk for further data analysis.

The temperature and the pressure sensors are fixed on top plate of experimental cell, but the portion of sensing element is able to decided arbitrary before the experiment starts. As a level of the experimental cell in the glass dewar can change, the distance from He II free surface to sensing elements can change.

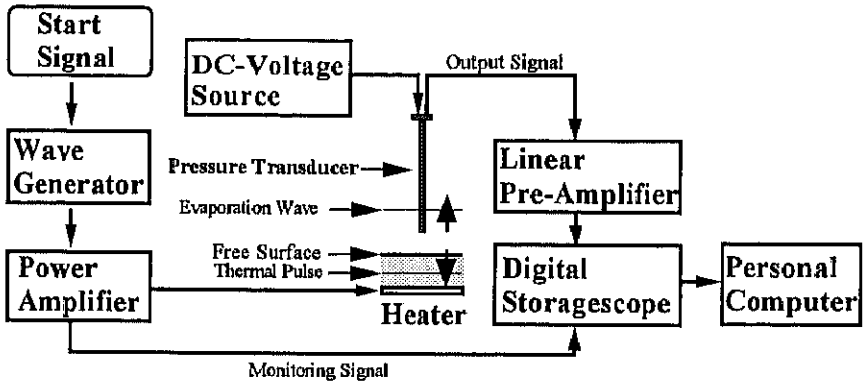

Fig. 3.16: The block diagram of the pressure measurement.

3.2 Visualization

The thermo-fluid dynamic phenomena in He II accompanied by appreciable density variation can be visualized with the aid of laser holographic interferometer as described by Iida et al.[50].

3.2.1 Laser holographic interferometer

Holography is one of the means to record an image of object using all the properties of light transmitted through an object. The essential properties of light are the intensity, the wavelength and the phase. Coherent light is necessary for making a hologram. It is characterized by invariable wavelength, amplitude and phase in both time and space. Some classes of laser light can satisfy the requirement of coherent light. They are capable of making an interference of two split light waves with some phase shifts from the same source, and of recording the phase content of the light wave. As the holography technique is applied to recording a fast phenomena such as a evaporation wave propagation in the present study, a double pulsed ruby laser with a very short pulse width of the order of $1\,ns$ should be utilized for minimizing the motion of object with respect to an optical system during the time interval between the first and second exposures. The above two features of the pulsed laser could solve any kinds of vibration problems which arise in the application of holographic interferometer. The installation of the laser on a vibration-isolation table

further ensures the vibration free operation. The wavelength of the ruby laser which is utilized for the present experiment is 694.3 nm. The optical arrangement of the laser holographic interferometer in the present study is shown in Fig. 3.17.

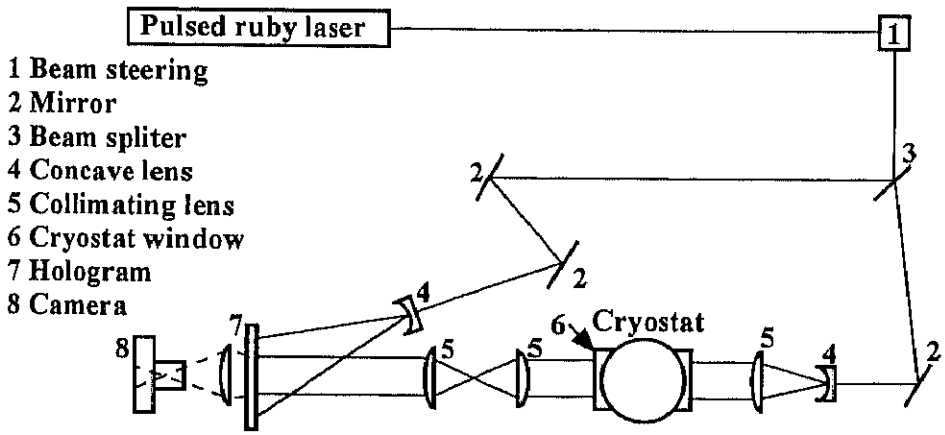

Fig. 3.17: The arrangement of optical element for the laser holographic interferometer.

In a holography application, a reference light wave interferes with an object one from the same source, and the phase difference signal between them is recorded on a hologram. Two hologram signals constructed by two separate exposures are recorded on a common hologram plate in the double exposure holography interferometer technique. In turn, two reconstructed light wave from two hologram sources on a hologram plate can produce interference fringes if there are any phase differences in the two hologram sources.

Some density variation in He II-vapor appears in the form of interference fringes with the holography interference system. The variation in the refractive index of He II-vapor due to the density variation in a evaporation wave gives the variation in optical path length along which laser light passes. In the present study, we applied both the finite-fringe and infinite-fringe methods complementarily. In the finite fringe method, parallel fringes are intentionally produced in a quiescent state by adjusting an optical element, and they are to be shifted according to the subsequent variation in the refractive index in question. In this mode the interval between

two adjoining fringes in a quiescent state is finite in contrast to infinite interval in the infinite fringe method. In the latter method the variation in the refractive index in a medium in question would cause the deflection of the reference fringes. And the amount of shift of a reference fringe can directly represent an approximate density profile of the evaporation wave in a local area.

The density can be approximately related to the refractive index, n, by

$$\frac{n-1}{n_0-1} = \frac{\rho}{\rho_0}, \tag{3.3}$$

where n_0 and ρ_0 are the refractive index and the density in the initial state, and n and ρ are the refractive index and density of the state of interest. This results in

$$\Delta n = \frac{n-1}{n_0-1}\Delta\rho. \tag{3.4}$$

Thus the density variation corresponding to one interference fringe is

$$\Delta\rho = \frac{\lambda\rho_0}{(n_0-1)\,L}\Delta X. \tag{3.5}$$

where ΔX and L are the number of interference fringe shift and the optical path length across the experimental cell ($60\,mm$) and λ is the wavelength of laser ($694.3\,nm$). The refractive index data of He II-vapor is given by thermo-physical properties software, HEPAC (CRYODATA INC.).

3.2.2 Cryostat and evacuation system

The photo of the metal type cryostat used in the visualization study is shown in Fig. 3.18. The cross-sectional view of the cryostat is also schematically shown in Fig. 19. This cryostat is cylindrical in shape and the height is about $100\,cm$ and the outer diameter is $50\,cm$, being made of stainless steel. The inside of the cryostat is evacuated down to $10^{-5}\,Pa$ for vacuum thermal isolation. There are the two tanks for liquid nitrogen for pre-cooling and auxiliary cooling. The liquid helium vessels are in the center portion of the cryostat. Three pairs of optical windows are seen in the illustration. The inner most windows installed in the He II vessel should

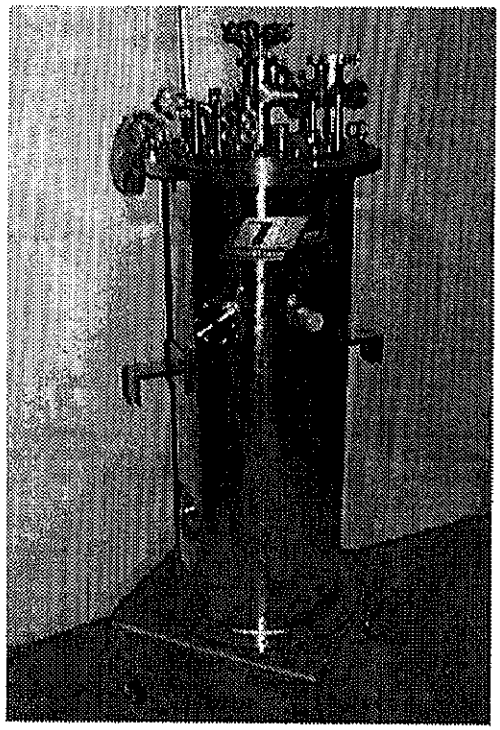

Fig. 3.18: The photo of the cryostat with optical windows for the visualization.

be of superleak-tight. The window glass plates at the intermediate stage maintained at the liquid nitrogen temperature are coated with IR absorbing thin film to absorb $300\,K$ thermal radiation as a potential parasitic heat leak through the windows. The outer most two are of vacuum tight. The experimental cell is located in the center portion of the cryostat. For recording a hologram, an expanded parallel laser beam pass through the experimental cell. The cell is a rectangular solid. There is a He II reservoir above the experimental cell for refill of He II into the experimental section and it functions as a thermal guard at liquid helium temperature. Another He II vessel below the shock tube is also equipped for thermal stabilization due to large thermal mass of He II. The vapor pressure in experimental section can be fine-controlled by the pressure control valves to keep the temperature constant there. The vapor pressure is measured by same pressure transducer utilized for the glass dewar experiment system. During a run of experiment, the temperature in the experimental section

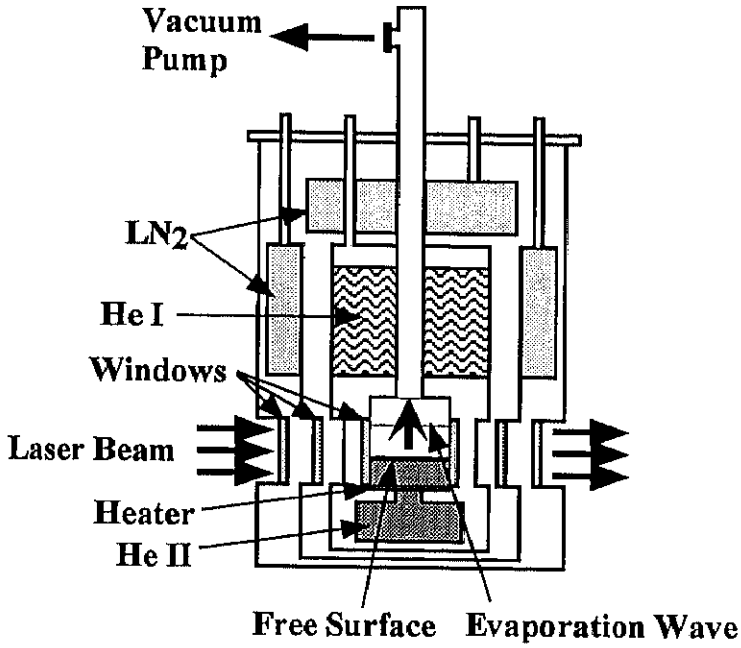

Fig. 3.19: The cross-sectional view of the cryostat with optical windows for the visualization.

is also kept constant with the pressure control system as described above. This cryostat can be used for experiments at the temperature down to $1.74\,K$ with a hold time around $2\,hours$.

3.2.3 Experimental cell

The experimental cell set in the cryostat is schematically shown in Fig. 3.20. The experimental cell for the visualization experiment is a rectangular solid, a width of $10\,mm$, a height of $37\,mm$, a length of $60\,mm$, quite similar to that for the temperature and pressure measurement. This experimental cell space is surrounded by two glass plates for visualization, and is enclosed by two adiabatic side walls and an adiabatic top plate of Bakelite. A planar Nichrom thin film heater ($30\,\Omega$) vacuum-deposited on a quartz glass substrate is located at the bottom of the cell.

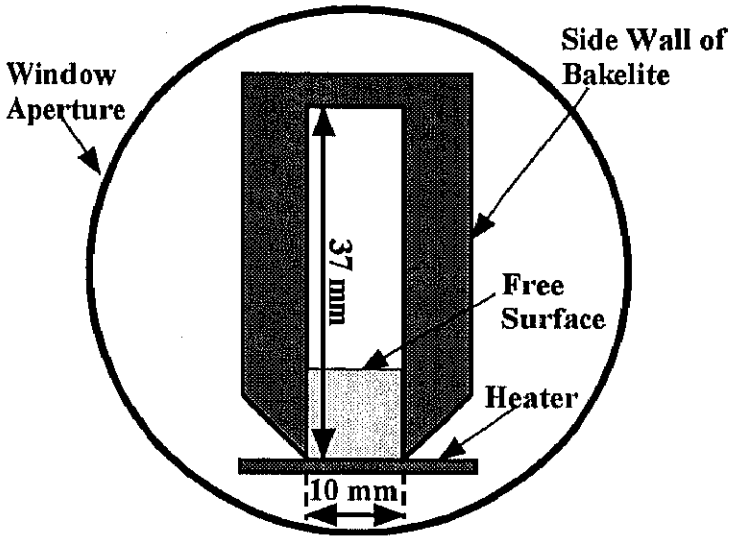

Fig. 3.20: The frontal view of the experimental cell in the cryostat for the visualization.

3.2.4 Procedure

The visualization block diagram are shown in Fig. 3.21. A double exposure technique is applied with a pulsed ruby laser ($694.3\,nm$, $10\,mJ$). The first exposure is made in an initial quiescent state. After that, the second exposure is done with an evaporation wave. The time interval between the onset of heating and the second flash of laser, t_D, ranges from several

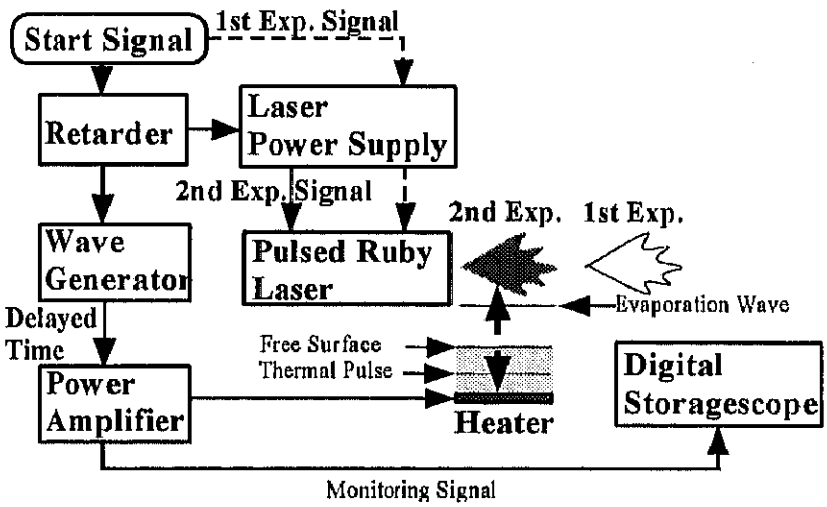

Fig. 3.21: The block diagram of the visualization.

hundred micro sec. to several milliseconds. A holographic information is recorded on a holographic plate, Agfa 10E75. In the image reconstruction process, a holographic plate is illuminated by a continuum He-Ne laser ($632.8\,nm, 5\,mW$) and a reconstructed holographic image showing a fringe field is photographed by a still camera. The detail of fringes are investigated for the density variation and the propagation speed of evaporation wave later.